Modeling the bacterial flagellum by an elastic network of rigid bodies

2011 Phys. Biol. 8 046009

(http://iopscience.iop.org/1478-3975/8/4/046009)

Phys. Biol. **8** (2011) 046009 (11pp) doi:10.1088/1478-3975/8/4/046009

Modeling the bacterial flagellum by an elastic network of rigid bodies

C Speier, R Vogel and H Stark

Institut für Theoretische Physik, Technische Universität Berlin, Hardenbergstr. 36, D-10623 Berlin, Germany

E-mail: christoph@itp.tu-berlin.de

Received 13 March 2011
Accepted for publication 27 June 2011
Published 20 July 2011
Online at stacks.iop.org/PhysBio/8/046009

Abstract

Bacteria such as *Escherichia coli* propel themselves by rotating a bundle of helical filaments, each driven by a rotary motor embedded in the cell membrane. Each filament is an assembly of thousands of copies of the protein flagellin which assumes two different states. We model the filament by an elastic network of rigid bodies that form bonds with one another according to a scheme suggested by Namba and Vondervistz (1997 *Q. Rev. Biophys.* **30** 1–65) and add additional binding sites at the inner part of the rigid body. Our model reproduces the helical parameters of the 12 possible polymorphic configurations very well. We demonstrate that its energetical ground state corresponds to the normal helical form, usually observed in nature, only when inner and outer binding sites of the rigid body have a large axial displacement. This finding correlates directly to the elongated shape of the flagellin molecule. An Ising Hamiltonian in our model directly addresses the two states of the flagellin protein. It contains an external field that represents external parameters which allow us to alter the ground state of the filament.

(Some figures in this article are in colour only in the electronic version)

1. Introduction

The bacterial flagellum is a biological locomotion machinery with components whose sizes range from the nanometer to the micrometer scale [1]. A rotary motor embedded in the cell membrane produces torque which a universal joint named hook transmits to a helical filament [2]. During the run mode of the bacterium, the motor rotates counter-clockwise. The left-handed helical filaments of several flagella form a rotating screw-like bundle. This induces a thrust force which pushes the bacterium forward [3]. So rotary motion of the motors is transformed into linear motion. If one motor reverses its sense of rotation, the attached filament leaves the bundle and goes through a sequence of different helical configurations, called polymorphic forms [1]. As a result, the bacterium tumbles, reorients itself and resumes linear motion when the filament joins the bundle again.

In order to increase food uptake, the bacterium can prolong the duration of the run phase between two short tumble phases when it swims along a chemical gradient [3]. The tumble phase and therefore the polymorphism of the flagellar filament are important in this motility scheme called chemotaxis to search for preferential conditions. In total 12 polymorphic shapes (two straight and ten helical forms) are predicted theoretically [4, 5] (see figure 1); most of them were observed in experiments [1] or synthesized by self-assembly [6].

In nature, the transition between polymorphic forms of the flagellum is triggered by reversing the rotational direction of the motor at the beginning of the tumble phase [1]. Shape transitions can also be induced by mechanical forces or torques applied to a flagellum [7, 8], by changing temperature [9], or by modifying solvent conditions such as pH value and salinity [10–12]. In order to address polymorphic transitions induced by pulling at a flagellum [12], we have used continuum theory and formulated an extended Kirchhoff rod model for the flagellar filament. With this model we could study the force-induced transition between the coiled and normal forms in detail [13]. Under normal conditions (pH value $\approx$7 and salinity $\approx$250 mM), the flagellum assumes the normal form (see figure 1). It has a left-handed helical shape and occurs during the run mode of the bacterium. This raises the question

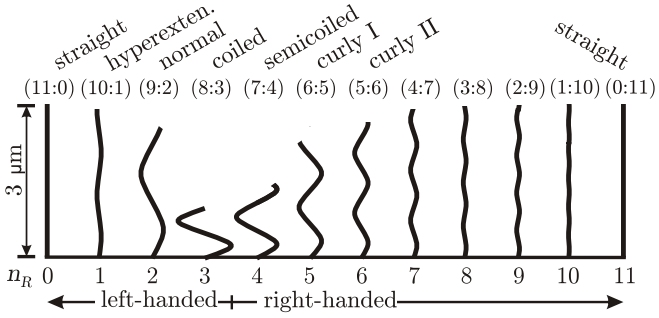

Figure 1. Illustration of the 12 polymorphic forms of the bacterial flagellum, after [12]. A piece of the filament with length 3 μm is shown. The total length ranges from 10 to 20 μm. The polymorphism number n_R gives the number of protofilaments in the R-state.

how the normal configuration is stabilized amongst the 12 possible polymorphic forms. In this paper, we contribute to answering this question by developing a coarse-grained model for the flagellar filament.

Surprisingly, nature only needs a single subunit, the protein flagellin, to realize different polymorphic forms of the filament. In section 2, we will review in detail how they arise from the two states R and L, which the subunit can assume. A major understanding of the flagellar polymorphism was developed in the 1970s by Asakura and Calladine based on experimental work [14] and mechanical modeling [4, 5, 15, 16]. The latter explained curvature and torsion of the helical configurations based on a circular arrangement of 11 protofilaments which can switch between a longer (L) and a shorter (R) type. Namba and Vondervistz used detailed structural information on the subunit to develop a scheme how neighboring flagellin molecules bind to one another [2]. With the help of this scheme, Hasegawa *et al* improved Calladine's predictions for curvature and torsion [17]. However, the models treated so far could not explain why the filament assumes a helical ground state. Srigiriraju and Powers introduced a continuum model and included an elastic mismatch strain between the inner and outer cores of the filament that ultimately stabilized one helical ground state [18, 19]. The special role of the normal polymorphic form and the molecular origin of the mismatch strain were not addressed. On the other hand, Kitao *et al* performed molecular dynamics (MD) simulations on atomic models of filament pieces and determined their helical parameters [20]. Coarse-grained MD simulations addressed rotating flagella [21]. Finally, Spagnolie and Lauga used slender body theory to show that the normal helical form is the most efficient one for bacterial propulsion [22].

In this paper, we present a coarse-grained model for the flagellar filament by introducing an elastic network of rigid bodies that interact via the characteristic binding scheme of Namba and Vondervistz [2]. In addition, an Ising Hamiltonian directly addresses the two states of the flagellin protein. With this idea we follow work by Wada and Netz who first employed the Ising model in modeling the flagellar filament [23]. Using Ising spins to describe internal states of macromolecular assemblies has a long tradition as shown by several early textbooks [24–26] and the seminal paper by Zimm and Bragg [27]. Recent applications can be found in [28–33].

Our coarse-grained model reproduces the helical parameters of the 12 polymorphic configurations very well. Most importantly, it suggests a mechanism on the molecular scale that produces an internal strain in the filament and stabilizes, in particular, the normal form. An external field in the Ising Hamiltonian represents external parameters and allows us to adjust the ground state of the filament. With our work we thus aim to contribute to answering the question posed by Calladine recently: 'What is the precise mechanism for determining which member of the family of 12 is to be built?' [34].

The paper is organized as follows. In section 2, we thoroughly review the structure of the bacterial filament. Section 3 presents our coarse-grained model for the bacterial filament including the Ising Hamiltonian and the elastic network of rigid bodies. In section 4, we analyze our model in two steps. We start with the elastic network and then present the results of the full model. We finish with the concluding section 5.

2. The bacterial flagellum

Understanding the polymorphism of the bacterial flagellum requires insight into the filament's molecular structure. The filament can be described by a circular arrangement of 11 protofilaments as illustrated by the cross-sectional view in figure 2. Each protofilament consists of flagellin proteins stacked onto one another [35] that can adapt two different states called L- and R-states [17]. X-ray structural analysis of both straight forms of the flagellum (see figure 1) reveals that all flagellin proteins in one protofilament are in the same state and that the repeat distances of the R- and L-type are, respectively, 5.186 and 5.267 nm [36–38]. Pure R-type and L-type protofilaments were already assumed by Calladine [4, 15, 16]; we refer to this fact as Calladine's rule [39]. Axial interactions along the protofilament that cause the highly cooperative behavior of the flagellin subunits to assume the same state were identified [38]. Finally, protofilaments of the same type cluster within the flagellum which is a natural outcome of Calladine's model [4, 5, 15, 16]. When same-type protofilaments are adjacent to one another, the number of mismatches and therefore elastic strain are reduced.

Neighboring protofilaments possess an axial displacement relative to one another depending on their R- or L-type. Since the protofilaments form a cylinder (see also the discussion in section 3.1), they have to be slightly tilted against the centerline of the flagellar filament. This creates the helical arrangement of the flagellin proteins and introduces a twist to the filament. Since protofilaments of L- and R-type have different lengths, they also bend the filament when both of them occur in the flagellum. So, 11 L-type protofilaments form a straight filament with an internal left-handed twist (see the polymorphic form (11:0) in figure 1). Increasing successively the number n_R of adjacent R-type protofilaments produces the 12 possible helical configurations of a bacterial flagellum with characteristic curvature κ and torsion τ. They are illustrated

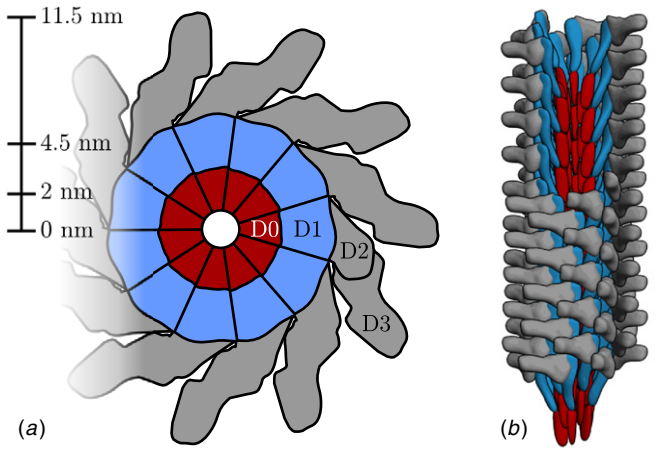

Figure 2. (*a*) Cross section of the flagellar filament. The four domains of flagellin define three nested tubes that describe the structure of the filament. The inner core of the filament colored in red is linked to the D0 domain of flagellin. The outer core defined by the D1 domain is colored blue and the outer tube formed by domains D2 and D3 is gray. (*b*) Side view of the flagellar filament shows how the flagellin proteins are stacked onto one another to form a protofilament.

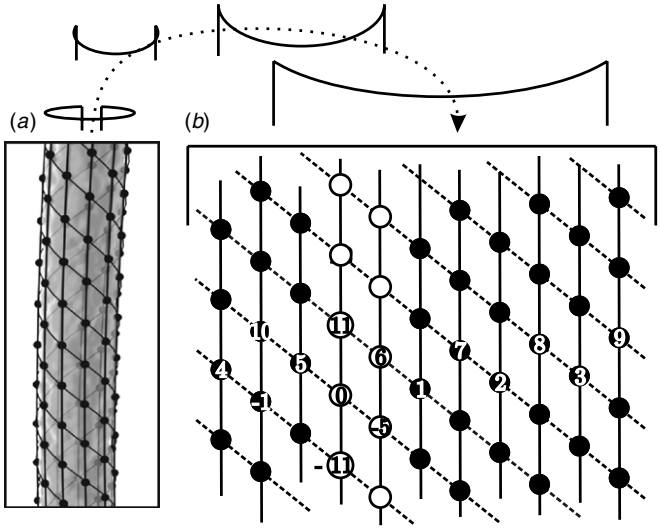

Figure 3. (*a*) Helical lattice on the surface of the filament, where dots indicate the flagellin molecules occupying the lattice sites. (*b*) The helical lattice folded up into a plane lattice. Along the 1-start helix the index of the lattice sites increases by 1. The full lines indicate 11-start helices which correspond to the protofilaments. The dashed lines show the five 5-start helices. The filament represents the normal helical form with two protofilaments being in the R-state (open circles), while the other nine protofilaments are in the L-state (closed circles).

in figure 1. For $n_R \geqslant 4$, the filament reverses its helicity and becomes right handed. In the swimming bacterium, the flagellum assumes the normal form, whereas during the tumbling phase semi-coiled, curly I and curly II forms occur [1]. Other configurations have been observed in experiments on isolated flagella taken from bacteria or reconstructed with mutants of flagellin molecules [6].

The flagellin protein consists of four domains. They determine the radial structure of the filament and describe it by three nested tubes (see figure 2). The inner tube or core has a radius of about 2 nm. In this area, the D0 domains of adjacent flagellin molecules bind to one another. Experiments showed that this domain does not change with the state of the protein. However, it plays a key role for realizing the helical shape of the filament [17]. The D0 domain causes different strains depending on the polymorphic forms. Reducing the associated strain energy then determines the helical ground state of the filament [40].

The intermediate tube or outer core lies around the inner core at a radius of about 4.5 nm. In this radial region, the D1 domains of flagellin proteins interact. Experiments demonstrated that the differences between the R- and L-states are mainly located in this part of the molecule [41]. It, therefore, determines the curvature and torsion of the filament's helical configurations [2]. Finally, D2 and D3 domains of the flagellin molecules define the outer tube. They are not important for forming the different polymorphic forms of the filament [2]. We therefore neglect them in our model.

3. Coarse-grained model

In this section, we present our coarse-grained model for the bacterial filament. It consists of two parts: we first introduce an Ising Hamiltonian to describe the two states of the flagellin molecule and their nearest-neighbor interactions. Secondly, we treat the flagellin protein as a rigid body that possesses binding sites, the locations of which depend on the flagellin state. We start with explaining the geometry of the filament.

3.1. Geometry of the filament

For modeling the filament it is essential to understand its geometry, which includes the relative positions of the flagellin proteins and directions along which they interact. Hence, we give here a short overview how the proteins form the helical lattice depicted in figure 3.

The positions of the flagellin molecules in the filament can be assigned to lattice points of a helical lattice that is situated on the outer core of the filament where the D1 domains are located. Helical means that there are no closed lines of lattice points when one goes around the cylindrical surface.

Figure 3 shows the lattice on the cylindrical surface of the filament and how it is opened to a plane lattice. There is one line of lattice points called 1-start helix that contains all these points. In figure 3(*b*), all the lattice points or flagellin molecules are labeled by an index. In the 1-start helix this index increases by 1 between neighboring lattice points. When one starts at a molecule with index i (e.g. $i = 0$ in figure 3(*b*)), the 1-start helix winds around the filament twice before it reaches the same protofilament at index $i + 11$. One can define further helices such as the 5-start, 6-start or 11-start helices. They are relevant for identifying directions along which the flagellin proteins interact with one another. The 11-start helices (full lines in figure 3(*b*)) contain molecules i, $i + 11$, etc and represent the 11 protofilaments. Along the five possible 5-start helices the index increases by 5. They are indicated by the dashed lines in figure 3(*b*).

Interactions between neighboring flagellin molecules along the 11-start and 5-start helices have been identified [35]. In particular, Samatey *et al* localized the interactions that lead to the highly cooperative behavior of the flagellin molecules along the protofilaments [38], in which all molecules are in the same state as described by Calladine's rule. Furthermore, we assume here that interactions along the 5-start helices cause protofilaments of the same type to cluster.

3.2. Part I: Ising Hamiltonian

The fundamental idea is to assign each flagellin at site i a spin variable σ_i that characterizes the state of the protein: $\sigma_i = 1$ represents the R-state and $\sigma_i = -1$ the L-state. The highly cooperative behavior along the protofilaments and also their clustering is achieved by introducing an Ising Hamiltonian with nearest-neighbor interactions along the 11-start and 5-start helices, respectively:

$$\mathcal{H}_I = -J_5 \sum_i \sigma_i \sigma_{i+5} - J_{11} \sum_i \sigma_i \sigma_{i+11} - H_0 \sum_i \sigma_i . \quad (1)$$

Here, J_5 and J_{11} indicate the strengths of interaction along the two directions in the helical lattice. In addition, we have also introduced an external-field term that favors, e.g., the R-state ($\sigma_i = 1$) over the L-state ($\sigma_i = -1$) when H_0 is positive. MD simulations by Kitao *et al* showed that at normal conditions hydrogen bonds are established in the filament that promote the L-state of flagellin in the filament [20]. However, if salinity or pH value of the solvent changes, these bonds are weakened such that the R-state flagellin is favored. Thus, the external field H_0 takes into account the varying external conditions from the solvent and should appear when modeling the polymorphism of the flagellum. In the following, we will assume that H_0 solely reflects the change of solvent conditions and its influence on the ground-state energy of the R- and L-states. We will not consider that other parameters of our modeling are influenced, such as spring constants, to describe bonds between binding sites in the following section.

So far, the Ising model implements Calladine's rule and leads to clustering of protofilaments of the same type. We have checked this by Monte Carlo simulations under the constraint that the total number of proteins in the R-state is fixed. However, without this constraint, the model only predicts a uniform ground state where all protofilaments are in the L- or R-state depending on the sign of H_0. This corresponds to the straight forms of the filament in figure 1. The normal helical form that is observed under normal conditions does not occur. We already mentioned that elastic strains in the D0 domain of flagellin molecules are responsible for observing helical polymorphic states. To allow for elastic strains, we therefore set up a rigid-body model for the flagellin molecules. They interact with their neighbors via bonds that form between distinct binding sites, the location of which is different in the L- and R-states.

3.3. Part II: rigid-body model for flagellin

In our rigid-body model for the flagellin, we follow work by Namba and Vonderviszt [2] who set up a characteristic binding scheme. Via distinct binding sites each molecule forms elastic bonds with its nearest neighbors. The L- and R-states of flagellin differ by the location of two of these binding sites. With their model, Namba and Vondervistz could reproduce curvature and torsion of the 12 possible polymorphic configurations of the flagellum [17]. In our model we have extended the binding scheme. As we will demonstrate in section 4.1, this proved to be crucial for stabilizing the normal configuration of the filament.

Table 1. Neighboring rigid bodies form bonds between specific binding sites. First column: labels of the binding sites of the central rigid body. (L) and (R) indicate the states when these bonds are active. Second column: index of the neighboring rigid body (according to figure 3) to which the central rigid body with index 0 forms a bond. Third column: binding site of the neighboring rigid body.

Central rigid body	Neighboring rigid body	Binding site
1	+5	4(L)/6(R)
2	−6	3(L)/5(R)
3(L)	+6	2
4(L)	−5	1
5(R)	+6	2
6(R)	−5	1
7	+1	8
8	−1	7

Figure 4(*a*) shows a short piece of the filament and in figure 4(*b*) one of its flagellin molecules is viewed from the side (top) and from the front (bottom). Rigid black arms emanate from a central black spot to the binding sites. Whereas the black backbone symbolizes the rigidity of the molecule, the transparent blue form should only give an impression of its silhouette but has no physical meaning for the model. The gray binding sites with labels 1 and 2 are present in both states of flagellin, while the red binding sites (labels 5, 6) are only activated in the R-state and the green sites (labels 3, 4) in the L-state. Table 1 summarizes the bonds that form between binding sites of a central flagellin and its neighbors. This is the binding scheme suggested by Namba and Vonderviszt. Figure 5 illustrates it for pure L-type (blue) and R-type (red) flagellin molecules. Our early investigations showed that the elastic network following from this binding scheme is unstable and collapses to a non-tubular form, like a balloon which loses its form after deflation [42]. The model is unstable against disturbances along the radial direction. For this reason we also include the interactions between the D0 domains of the flagellin proteins in the inner core of the filament. We already mentioned that they are also crucial for realizing the helical configurations of the filament [35]. In figure 4(*b*), the corresponding inner binding sites are labeled by 7 and 8. They form bonds with neighboring molecules along the 1-start helix as summarized in table 1. With this extension the elastic network relaxes into its stable ground state at a given spin configuration $\{\sigma_i\}$.

The figure caption of figure 4 contains a detailed description of the model parameters. We stress here the distance E between the neutral binding sites 1, 2 and the distances Q_L, and Q_R of the state-specific binding sites 3,

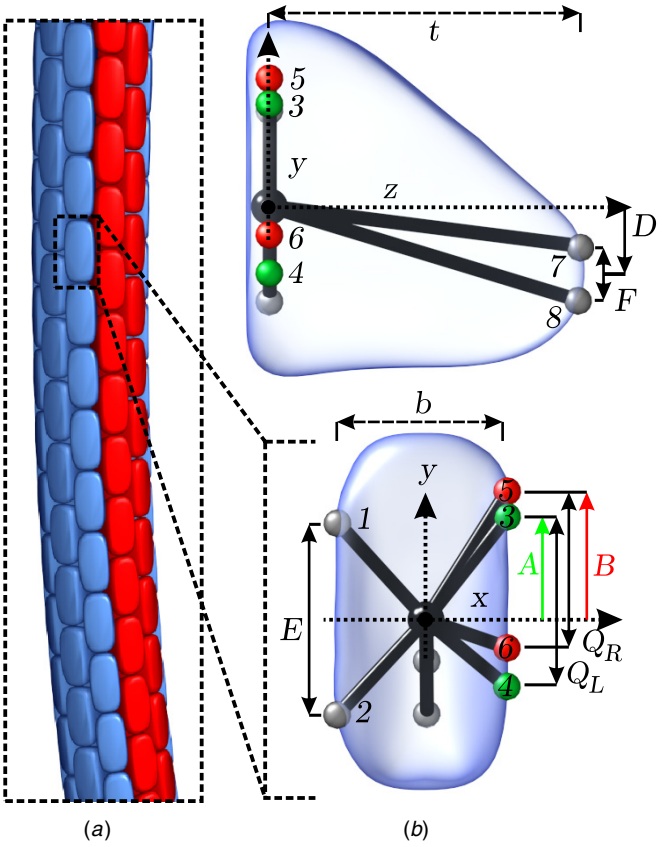

Figure 4. (*a*) A microscopic view of a short piece of the filament shows the arrangement of the model flagellins in the protein network. (*b*) One model flagellin viewed from the side (top) and from the front (bottom). Rigid black arms emanate from a central black spot to neutral binding sites 1, 2, 7, and 8, which exist in both states of the flagellin. The green sites 3, 4 and the red sites 5, 6 are only activated in the L- and R-state, respectively. The blue transparent surface only symbolizes the borders of the rigid body. The central black spot is also the origin of a Cartesian coordinate system attached to the rigid body. The origin lies in the plane of binding sites 1–6 and its horizontal position is in the middle between sites 1, 2 and 3–6. The y coordinates A and B define the respective axial positions of the binding sites 3, 5 and thereby the internal twist of the pure L- or R-form of the filament. The distance between the two binding sites 3, 4 and 5, 6 are given by Q_L and Q_R, respectively. The distance between sites 1, 2 is E and their y coordinates are $E/2$ and $-E/2$. The inner binding sites 7, 8 are characterized by the axial displacement or y coordinate D of their center and their distance F. For further use, we define the difference $C = Q_L - Q_R$, which is the difference in length of the flagellin in the L- and R-state. Finally, b and t are the width and depth of the model molecule.

4 and 5, 6. Furthermore, A and B are the axial positions or y coordinates of binding sites 3 and 5. Figure 5 illustrates how pure L-type (blue) and R-type (red) rigid bodies pack together and form bonds with their neighbors along the 5-start and 6-start directions. The bonds, in the D1 domain, always form between a neutral and an active binding site. From the schematic drawings one recognizes that $E+Q_L$ and $E+Q_R$ are the repeat distances in the L-type and R-type protofilaments, respectively. Therefore, $C = Q_L - Q_R$ is the difference in length of the flagellin molecule in the L- and R-states. Finally, the axial positions A and B of the green and red binding sites determine the tilt angles of the rigid-body assembly relative

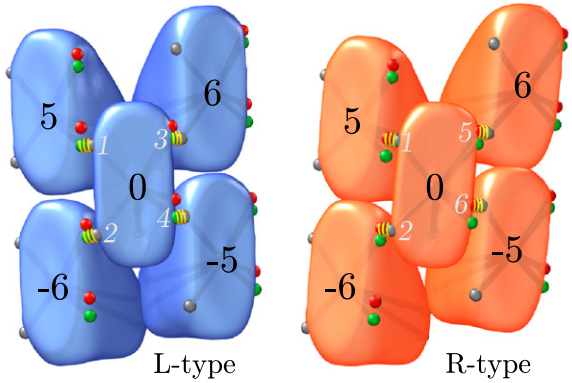

Figure 5. Assembly of L-type (blue) and R-type (red) rigid bodies in the filament. In the L-state the green binding sites are active, in the R-state the red sites are switched on. They always form bonds to the neutral gray binding sites along the 5-start and 6-start directions. Due to the different axial positions of the green and the red pairs of binding sites, a different internal twist occurs in the straight filaments of pure L-type and R-type protofilaments. The different distances between the binding sites in each pair cause different lengths of the flagellin molecules and therefore of the L-type and R-type protofilaments. If the domain of L-type rigid bodies on the left meets the domain of R-type rigid bodies on the right, the active binding sites 3, 4 do not match with the neutral binding sites 1, 2. Therefore, elastic deformations occur in the domain wall, the energy of which is described by the Hamiltonian $\mathcal{H}_{\mathrm{RB}}$ of equation (2).

to the central axis of the filament and, therefore, the internal twist.

The rigid body model for the flagellin molecule is characterized by the width b and depth t of the molecule and the six parameters A, B, C, D, E and F to position the binding sites. Some of them follow directly from experimentally determined values. The rigid bodies are packed in a hendecagon (11-sided polygon) similar to the schematic picture in figure 2(*a*). For the distance of the outer binding sites to the filament's center we take 4.5 nm which is typically given as the radial position of the D1 domain [37]. Then, the depth of the rigid bodies is $t = 4.5\cos(\pi/11)$ nm $= 4.318$ nm. The width is the side length of the hendecagon, so $b = 2 \cdot 4.5\sin(\pi/11)$ nm $= 2.536$ nm. We also choose the experimentally determined values for the parameter $C = 0.081$ nm and for the repeat distances of proteins in a protofilament in the R-state, $E+Q_R = 5.186$ nm, and in the L-state, $E + Q_L = 5.267$ nm [35]. So when E is chosen, we can calculate the parameters Q_R and Q_L. Besides E also the parameters A, B, D and F have to be chosen, on which we will comment in section 4.1.

The rigid bodies establish bonds with their neighbors along the 1-start, 5-start and 6-start helices and form an elastic network. We assign each binding site m in the rigid body i a position vector $\boldsymbol{r}_{mi}$. Whenever two binding sites are not in contact, a harmonic spring force acts such that the total energy of the elastic network becomes

$$\mathcal{H}_{\mathrm{RB}} = \frac{1}{2} \sum_{\langle ij(mn)(\sigma)\rangle} k_{mn}(\boldsymbol{r}_{mi} - \boldsymbol{r}_{nj})^2. \qquad (2)$$

The symbol $\langle ij(mn)(\sigma)\rangle$ means that for each nearest-neighbor pair of rigid bodies (i, j), the appropriate bond between sites m and n is chosen whose locations depend on the spin states σ_i

and σ_j. In the following we only distinguish spring constants for bonds in the outer core, $k_{mn} = k_O$, and in the inner core $k_{mn} = k_I$.

4. Results

We analyze our model in two steps. We first concentrate in section 4.1 on the elastic energy $\mathcal{H}_{\mathrm{RB}}$ of the network of rigid bodies since this energy mainly determines the configuration of the filament.

During the analysis in section 4.1, we assume Calladine's rule to be fulfilled and protofilaments of the same type to cluster such that only the 12 polymorphic forms of figure 1 occur for which we determine curvature, torsion and elastic energy. In section 4.2, we then perform Monte Carlo simulations for the full model taking into account the Ising Hamiltonian of equation (1) and determine the spin state of the flagellin proteins from the simulations. For appropriate choices of parameters, Calladine's rule and the clustering of same-type protofilaments indeed occur. Furthermore, we demonstrate that with the 'external field' H_0 one can tune the ground state of the filament to a specific polymorphic form.

4.1. Analysis of the rigid-body network

The principal idea is the following. We set up the spin states of the rigid bodies according to the 12 polymorphic forms of figure 1. For each of these helical forms we then determine curvature and torsion of the ground state by minimizing the elastic energy $\mathcal{H}_{\mathrm{RB}}$ with the help of a gradient-descent method where positions and orientations of the rigid bodies are allowed to relax. The appendix explains how we extract the filament's curvature and torsion from the positions of the rigid bodies. All the simulations in this and the following section were done for filament fragments of 110 subunits with open ends. This means that subunits at the border of the filament fragment exhibit free dangling bonds, which do not exert forces. The fragments have a length of approximately 0.05 μm which corresponds to 1/200 of a full-length filament. We minimized the elastic energy for filament fragments with a few thousand subunits and confirmed that finite-size and boundary effects are negligible.

Our model still contains parameters which do not correspond directly to experimentally known values. In the following we carefully study their influence. In the end, it will turn out that the displacement D of the pair of inner binding sites is the crucial parameter in our model. We start with choosing the parameters D, E and F and first set $D = 0$ nm. For the distance of the state-independent outer binding sites we take $E = (Q_L + Q_R)/2 = 2.613$ nm, where the value follows from the measured respective lengths of the R- and L-state flagellin [37], $E + Q_R = 5.186$ nm and $E + Q_L = 5.267$ nm. The inner binding sites of 11 rigid bodies are stacked onto one another when walking along the 1-start helix (see figure 3(*b*)) to reach the same protofilament. The distance F of these binding sites does not depend on the flagellin state, so we choose an average value $F = (2E + Q_R + Q_L)/(2 \cdot 11) = 5.227/11$ nm.

Furthermore, we have the spring constants k_O and k_I of the outer and inner bonds. Since the absolute value of the elastic energy is not relevant in this section, we give the energy in terms of k_O times the square of a characteristic length and choose k_I relative to k_O. Finally, we need the positions A and B of the state-dependent binding sites (see figure 4(*b*)). We calibrate their values such that the twist of the relaxed rigid-body network in the pure L- and R-states corresponds, respectively, to the measured values of pure L- and R-state flagellar filaments, namely $\tau_L = -5.62\ \mu\mathrm{m}^{-1}$ and $\tau_R = 13.45\ \mu\mathrm{m}^{-1}$ [37]. This calibration is repeated whenever a parameter is changed.

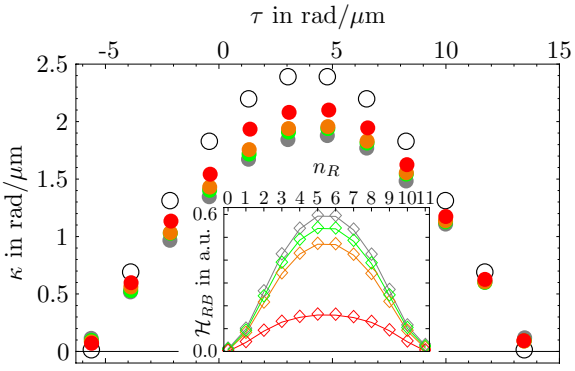

Figure 6. Curvature κ versus torsion τ as a result of minimizing elastic energy $\mathcal{H}_{\mathrm{RB}}$ for a given number n_R of adjacent R-state protofilaments. Colors indicate different strengths k_I of the inner bonds in units of k_O of the outer bonds: red: $k_I = k_O/20$, orange: $k_I = k_O/2$, green: $k_I = k_O$, and gray: $k_I = 2k_O$. Further parameters are $D = 0$ nm, $E = 2.613$ nm and $F = 5.227/11$ nm. The open circles are the helical parameters from Calladine's model [5]. Inset: elastic energy in arbitrary units as a function of n_R.

In figure 6, we plot curvature versus torsion for the 12 polymorphic states. The different colors show results when the strength of the inner bonds varies from strong (gray: $k_I = 2k_O$) to weak (red: $k_I = k_O/20$) relative to the outer spring constant. The open circles are the helical parameters from Calladine's model ($\kappa = 2.4\ \mu\mathrm{m}^{-1} \sin(\pi n_R/11)$ and $\tau = \tau_L + (\tau_R - \tau_L)n_R/11$) [5]. Our results are closest to these values if the inner bonds are much weaker than the outer ones. We therefore choose $k_I = k_O/20$ in the following. However, we still do not reach the curvature values from Calladine's model. We will address this fact below.

The inset of figure 6 shows elastic energy in arbitrary units as a function of the number n_R of R-state protofilaments. For all spring constants k_I, both straight filaments, either in the L- or R-state, correspond to energetical ground states. All helical configurations with non-zero curvature, including the normal form observed in nature, are energetically unfavorable. Note that this conclusion does not change when we include the spin interaction energy of the Hamiltonian $\mathcal{H}_I$ since the energy of the curved filaments would further increase due to the domain walls between clusters of L- and R-state protofilaments.

In order to stabilize the normal configuration as the energetical ground state, we have three parameters to vary: E, F, and D. We checked that reasonable variations in the distances of the outer neutral (E) and the inner (F) binding sites do not influence our results so far. However, the axial displacement D of the inner binding sites has a striking effect. In figure 7, we plot elastic energy in arbitrary units as a function

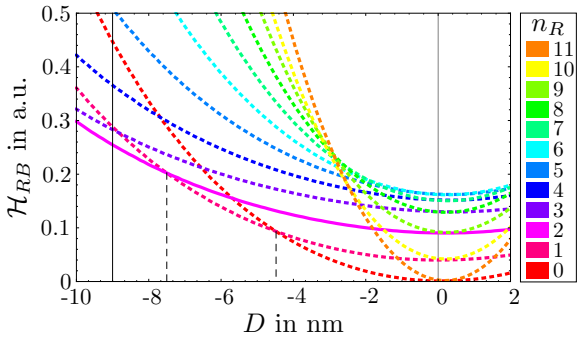

Figure 7. Elastic energy in arbitrary units as a function of the axial displacement D of the inner binding sites for all the polymorphic forms characterized by n_R. The vertical dashed lines indicate where the stability changes from the straight to the hyperextended and to the normal state when D decreases. The full vertical intersects the energy functions at $D = 9$ nm. The parameters are $k_I = k_O/20$, $E = 2.613$ nm and $F = 5.227/11$ nm.

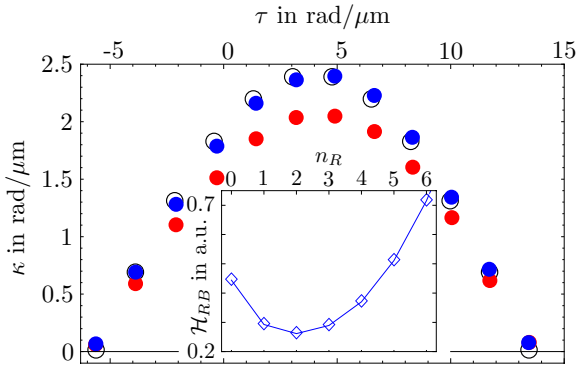

Figure 8. Curvature κ versus torsion τ for the different polymorphic forms for $D = -9$ nm. Red dots: $C = 0.081$ nm, blue dots: $C = 0.094$ nm. Other parameters are $k_I = k_O/20$, $E = 2.613$ nm, and $F = 5.227/11$ nm. The open circles are the helical parameters from Calladine's model [5]. Inset: elastic energy in arbitrary units as a function of n_R for $C = 0.094$ nm.

of D for the different polymorphic forms characterized by n_R. The energy values at $D = 0$ correspond to the curve in the inset of figure 6 for $k_I = k_O/20$. Choosing a non-zero D breaks the symmetry between n_R and $11 - n_R$ R-state protofilaments. Up to values of D around -4.5 nm the pure L-state filament is the ground state. Then, the hyperextended filament ($n_R = 1$) becomes stable and for D smaller than -7.5 nm the normal state becomes energetically favored. In the discussions in section 5 we will demonstrate that this result is in agreement with the elongated shape of the real flagellin protein.

For $D = -9$ nm we plot in figure 8 curvature κ versus torsion τ for all polymorphic forms (red dots). Still, the curvature values are below the values from Calladine's model [5].

We start our simulations on pure L- and R-type filaments with the input parameter $C = 0.081$ nm. This is the length by which the repeat distances in the L- and R-type filaments differ in real flagella. However, in order to reduce strains within the filament, the L- and R-type protofilaments relax during the simulations to repeat distances of their subunits that differ by a length smaller than 0.081 nm. Only when we increase the input parameter to $C = 0.094$ nm, do our simulations on pure filaments result in repeat distances that differ by the correct value of 0.081 nm observed in experiments. With the corrected input parameter C, we then obtain very good agreement with Calladine's model [5] as illustrated by the blue dots in figure 8. Finally, the inset demonstrates again for the corrected parameter C that the normal form is energetically favored with respect to the other configurations.

In a next step we performed Monte Carlo simulations including the spin state of the flagellin proteins in order to check if the elastic energy $\mathcal{H}_{\mathrm{RB}}$ alone is sufficient for stabilizing the 12 polymorphic forms of the Calladine model and, in particular, the normal state. We start with a random spin configuration of the rigid bodies, perform a spin flip and for the resulting spin configuration minimize $\mathcal{H}_{\mathrm{RB}}$ further with several gradient-descent steps. The outcome of this procedure was that we neither observed protofilaments with rigid bodies in one state (Calladine's rule) nor the clustering. Thus, the Hamiltonian $\mathcal{H}_{\mathrm{RB}}$ of the rigid-body network does distinguish the 12 polymorphic forms by their energy, but does not stabilize these 12 forms. So it was necessary to extend our model by the Ising Hamiltonian $\mathcal{H}_I$ of equation (1).

4.2. Analysis of the full model with Monte Carlo simulations

We now use the full Hamiltonian consisting of the Ising Hamiltonian and the energy of the rigid-body network

$$\mathcal{H}_F = \mathcal{H}_{\mathrm{RB}} + \mathcal{H}_I. \tag{3}$$

As discussed in section 3.2, $\mathcal{H}_I$ enforces Calladine's rule and clustering of same-state protofilaments by choosing sufficiently large interaction strengths along the 11-start (J_{11}) and the 5-start (J_5) helices, respectively. The external field H_0 adjusts the polymorphic ground state.

Our goal was not to present here a systematic parameter study of the full model. Instead, we performed many simulations to adjust the interaction strengths J_5 and J_{11} to sufficiently large values such that Calladine's rule and the clustering occurred. In addition, the outer spring constant k_O was chosen sufficiently large such that $\mathcal{H}_{\mathrm{RB}}$ dominates the full energy and the absolute minimum at the normal state configuration is preserved. This procedure led to the following choice of parameters: $J_5 = 1\,k_BT$, $J_{11} = 10\,k_BT$, $k_O = 660\,k_BT/(\mathrm{nm})^2$ and $k_I = k_O/20$, where k_{BT} is the thermal energy. A large J_{11} makes sense to enforce uniform protofilaments. On the other hand, J_5 cannot be too large, otherwise all helical states would be suppressed when domain walls between L- and R-type protofilaments cost too much energy.

With this choice of parameters, the parameters mentioned in figure 8 including the corrected value $C = 0.094$ nm, and various external-field values H_0 we performed Monte Carlo simulations. Curvature and torsion for the resulting helical conformations are illustrated in figure 9. Every point in the plot indicates an individual simulation run, which was started from a random spin configuration. The blue points belong to $H_0 = 0\,k_BT$. During all the simulation runs the filaments relaxed into the helical form of the normal state with torsion and curvature very close to the values predicted by Calladine's

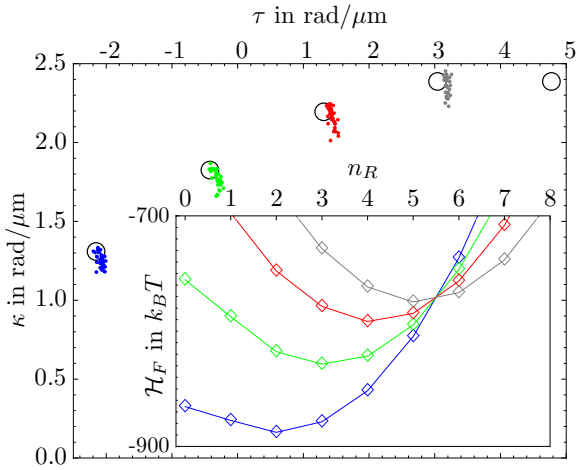

Figure 9. Curvature κ versus torsion τ as a result of the Monte Carlo simulations for the full model. Each point is the result of one simulation run. Colors indicate different strengths of the external field: blue: $H_0 = 0\,k_BT$, green: $H_0 = 1\,k_BT$, red: $H_0 = 2\,k_BT$ and gray: $H_0 = 3\,k_BT$. Other parameters are chosen as indicated in the text. The open circles are the helical parameters from Calladine's model [5]. Inset: full energy $\mathcal{H}_F$ as a function of n_R calculated for perfect spin realizations of the polymorphic forms.

model (open circles). The blue curve in the inset shows the full energy $\mathcal{H}_F$ as a function of n_R when we assume perfect spin realizations of the polymorphic forms. It is similar to $\mathcal{H}_{\mathrm{RB}}(n_R)$ in the inset of figure 8 confirming that $\mathcal{H}_{\mathrm{RB}}$ dominates the full energy for $H_0 = 0\,k_BT$. Only the energy of the pure L-state filament is shifted downwards relative to the other energy values since an energy cost for domain walls between L- and R-state protofilaments does not have to be included.

The flagellar filament assumes other polymorphic forms when salinity and pH value of the solvent are changed as demonstrated, for example, by Darnton and Berg [12]. In our model, the observed ground state can be adjusted by the external field H_0. This is illustrated by further simulation results in figure 9. When we increase the external field starting from $H_0 = 0\,k_BT$ (blue dots) over $H_0 = 1\,k_BT$ (green), $H_0 = 2\,k_BT$ (red) to $H_0 = 3\,k_BT$ (gray), the filament assumes the sequence of normal, coiled, semi-coiled and curly I forms. A non-zero H_0 effectively introduces an energy term linear in n_R with negative slope. So with increasing H_0, the ground state of the filament is shifted to larger n_R as the inset of figure 9 demonstrates. This feature makes clear why we can identify the external field H_0 with external parameters such as salinity or pH value of the solvent in order to induce a transformation of the filament from one polymorphic form to a neighboring state. In particular, during the transition from $n_R = 3$ to $n_R = 4$ also the sign of chirality switches which should be accompanied by a large energetic barrier. So our investigations only address the ground-state energies of the different polymorphic forms and not how they transform into one another. The lines in the inset of figure 9 are only guide to the eyes. We have addressed the kinetics of polymorphic transitions in [13]. Finally, we mention that the Monte Carlo simulations only give a few data points in the $\kappa - \tau$ region occupied by the inset in figure 9. They describe states which are caught in local minima of the complex energy landscape.

5. Discussion and conclusion

In this paper, we have modeled the flagellar filament by an elastic network of rigid bodies that interact via a characteristic binding scheme suggested by Namba and Vonderviszt [2]. In addition, by introducing inner binding sites of the rigid bodies, we can not only stabilize the elastic network, but also have the means to tune energy such that the normal filament configuration becomes the energetical ground state. Our modeling suggests an elongated shape of the flagellin molecule in accordance with its real shape, as we demonstrate below. An additional Ising spin variable referring to the L- and R-states, respectively, and a typical spin interaction energy are needed to observe Calladine's rule and the clustering of same-type protofilaments. An 'external' field in the spin Hamiltonian allows us to adjust the energy difference between the R- and L-state realization of flagellin and thereby the ground state of the filament. It describes the influence of external parameters such as salinity or pH value of the solvent.

The original model by Namba and Vondervistz has two main ingredients [2]. They approximate the flagellin protein as a rigid body due to the presence of α-helices in the D0 and D1 domains. Furthermore, they introduce the specific binding scheme such that protofilaments of different type have different lengths and that adjacent protofilaments display a state-dependent axial displacement. Kitao *et al* indeed found in MD simulations that the D1 domain of flagellin is significantly rigid, while the D0 domain is more flexible [20] which we consider in our modeling by the small spring constant of the inner bonds. Their MD simulations and recent experiments [40] demonstrate differences in the overall shape (tertiary structure) of R- and L-type flagellin molecules. However, the two states of the protein mainly differ in position and orientation within the filament. Most importantly, Kitao *et al* identified so-called sliding interactions between binding sites that differ in their location in the R- and L-type proteins. This corresponds to the essential feature in the binding scheme of the Namba–Vondervistz model [2].

In our model proteins, the inner binding sites form bonds along the 1-start helix. This is certainly a simplification of the real situation. Several authors have stressed that release of strain between the inner (D0) and outer (D1) domains of flagellin determines the helical ground state of the filament [2, 19, 35, 39, 40]. The most important result of our work is that the axial distance between the inner and outer binding sites reveals the mechanism via which the associated stress is produced and released. We will discuss this mechanism below. It only depends on the overall shape of the flagellin protein and does not rely on molecular details. In figure 10(*a*), we present a representation of the real flagellin protein produced from data of its atomic positions [35]. We also superimpose our model protein with an axial displacement of 9 nm between inner and outer binding sites which was necessary to stabilize the normal form of the filament. There is a remarkable agreement between the elongated shape of flagellin and our model protein.

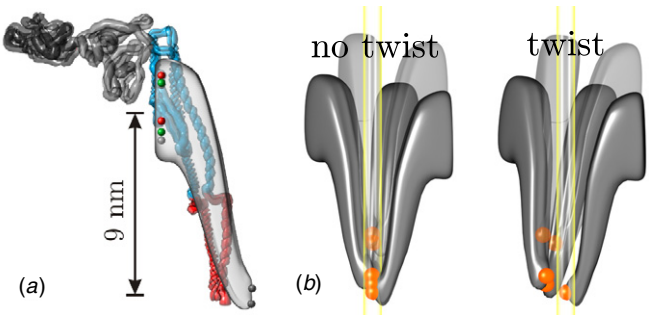

Figure 10. (*a*) Tertiary structure of the flagellin protein constructed with atomic positions of the R-type flagellin from [35] and our model protein superimposed. The elongated shape of the D0 (red) and D1 (blue) domains of the flagellin molecule coincides with the axial distance of the inner and outer binding sites in the model protein. (*b*) Arrangement of model proteins in filaments without twist (left) and with twist (right). Note the large deflection of the inner binding sites from the central axis when twist is present. Dark gray: three model proteins along a 1-start helix; light gray: two model proteins from a neighboring 1-start helix.

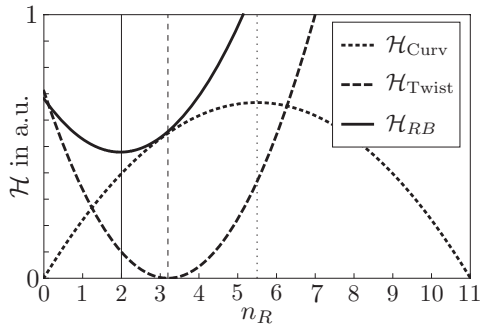

Figure 11. Mechanism for generating the normal form as ground state. The total elastic energy (full line) is decomposed into two harmonic parts. The concave bending energy (dotted line) is maximal for maximum curvature between curly I ($n_R = 5$) and curly II ($n_R = 6$) states and zero for straight filaments. The convex torsional energy (dashed line) is zero for zero τ between the coiled ($n_R = 3$) and semi-coiled ($n_R = 4$) states. By adjusting the curvature of both energies accordingly, the minimum of the total energy (full line) can be placed at the normal state.

We note that with their original binding scheme Namba and Vondervistz could successfully calculate curvature and torsion of the different polymorphic configurations within a coarse-grained model that does not rely on molecular details. In particular, the binding sites of the rigid bodies cannot be remapped on an all-atom representation of flagellin. Extending this successful coarse-grained model, we could identify that the elongated shape of flagellin favors a helical ground state.

Now we ask the question how this elongated shape favors the helical ground state? We know from the results in figure 6 that a filament built from our model protein with a more compact shape, which means axial distance $D = 0$ nm, has the largest elastic energy when curvature is the largest. Thus, straight filaments are favored. On the other hand, straight filaments with internal twist built from elongated model proteins contain internal stress. This is illustrated in figure 10(*b*). On the left-hand side the model proteins are arranged without twist and the inner binding sites stack onto one another along the central axis with little cost of elastic energy. If the filament possesses an internal twist, the inner binding sites are strongly deflected from one another and from the central axis when the axial displacement D is large (picture on the right). This produces large stresses within the model proteins or a large elastic energy for high twists. In order to relax it, the filament assumes a helical ground state as a compromise with reduced torsion and some curvature. We illustrate the main mechanism in figure 11. The total energy (full line) of the filament consists of two parts which we assume in their simplest approximation to be harmonic functions in the relevant variable, the number n_R of R-state protofilaments. The concave bending energy (dotted line) is largest when curvature is largest between the curly I ($n_R = 5$) and curly II ($n_R = 6$) configurations and zero for the straight filaments. The convex torsional energy (dashed line) is zero for zero τ between the coiled ($n_R = 3$) and semi-coiled ($n_R = 4$) forms and grows quadratically in $\tau \propto n_R$. Adjusting both energies appropriately gives a minimum total energy at the normal state, i.e. $n_R = 2$.

Despite the fact that we disregard a lot of molecular details in our modeling following the path of Namba and Vondervisz [2], we are able to present a mechanism related directly to the shape of the flagellin molecule via which the flagellar filament selects its helical ground state. This confirms the common view [2, 19, 35, 39, 40] that the L- and R-states of the outer (D1) domain of flagellin enable the formation of the different polymorphic forms of the flagellum, whereas the inner (D0) domain plays a crucial part in selecting the energetically preferred helical configuration.

Acknowledgment

We thank the Deutsche Forschungsgemeinschaft for financial support through the research training group GRK1558.

Appendix A. Curvature and torsion of the rigid-body network

The rigid-body networks of the model proteins exhibit helical forms. We describe here how we determine their curvatures and torsions from the position vectors $\boldsymbol{r}_i$ of the centers of the rigid bodies indicated by the central black spheres in figure 4(*b*).

First, we introduce a unit tangent vector to the filament at subunit or model protein i. We define the difference vectors to neighbor proteins in the same protofilament, $\boldsymbol{r}_{i+j+11} - \boldsymbol{r}_{i+j}$, average them along a 1-start helix over all 11 protofilaments and normalize the resulting vector:

$$\boldsymbol{t}_i = \frac{\sum_{j=-5}^{5}(\boldsymbol{r}_{i+j+11} - \boldsymbol{r}_{i+j})}{|\sum_{j=-5}^{5}(\boldsymbol{r}_{i+j+11} - \boldsymbol{r}_{i+j})|}. \tag{A.1}$$

The curvature of a space curve is calculated from the derivative of the tangent vector with respect to its arc length s, $\kappa = |\mathrm{d}\boldsymbol{t}/\mathrm{d}s|$. Discretizing the derivative gives the local curvature κ_i at location $\boldsymbol{r}_i$:

$$\kappa_i = \frac{|\boldsymbol{t}_{i+11} - \boldsymbol{t}_i|}{|\boldsymbol{r}_{i+11} - \boldsymbol{r}_i|}. \tag{A.2}$$

The torsion of a rod is defined by $\tau = \mathrm{d}\alpha/\mathrm{d}s$. Here, $\mathrm{d}\alpha$ is the angle by which the cross section of the rod is rotated about its tangent $\boldsymbol{t}$ when one proceeds a distance ds along the rod. Assuming small changes along one protofilament, we determine $\mathrm{d}\alpha_i$ by the cross product of the radial unit vectors $\boldsymbol{e}_i^z$, $\boldsymbol{e}_{i+11}^z$ of neighboring subunits in one protofilament (indicated by the z axis in figure 4(*b*)) and project it onto the local tangent vector $\boldsymbol{t}_i$. Thus, the local torsion τ_i becomes

$$\tau_i = \frac{\left(\boldsymbol{e}_i^z \times \boldsymbol{e}_{i+11}^z\right) \cdot \boldsymbol{t}_i}{|\boldsymbol{r}_i - \boldsymbol{r}_{i+11}|}. \tag{A.3}$$

Finally, we determine the curvature κ and the torsion τ of the model filament consisting of N subunits by averaging over the local values of the 11 most centrally located subunits:

$$\kappa = \sum_{N/2-5}^{N/2+5} \kappa_i, \qquad \tau = \sum_{N/2-5}^{N/2+5} \tau_i. \tag{A.4}$$

This algorithm has been tested at model filaments with known curvature and torsion.

References

[1] Berg H C 2003 *E. coli in Motion (Biological and Medical Physics, Biomedical Engineering)* (Berlin: Springer)

[2] Namba K and Vonderviszt F 1997 Molecular architecture of bacterial flagellum *Q. Rev. Biophys.* **30** 1–65

[3] Turner L, Ryu W S and Berg H C 2000 Real-time imaging of fluorescent flagellar filaments *J. Bacteriol.* **182** 2793–801

[4] Calladine C 1978 Change of waveform in bacterial flagella: the role of mechanics at the molecular level *J. Mol. Biol.* **118** 457–79

[5] Calladine C R 1983 Construction and operation of bacterial flagella *Sci. Prog.* **68** 365–85

[6] Kamiya R, Asakura S and Yamaguchi S 1980 Formation of helical filaments by copolymerization of two types of 'straight' flagellins *Nature* **286** 628–30

[7] Hotani H 1982 Micro-video study of moving bacterial flagellar filaments: III. Cyclic transformation induced by mechanical force *J. Mol. Biol.* **156** 791–806

[8] Macnab R and Orston M 1977 Normal to curly flagellar transitions and their role in bacterial tumbling—stabilization of an alternative quaternary structure by mechanical force *J. Mol. Biol.* **112** 1–30

[9] Hasegawa E, Kamiya R and Asakura S 1982 Thermal transition in helical form of salmonella flagella *J. Mol. Biol.* **160** 609–21

[10] Kamiya R and Asakura S 1976 Helical transformations of salmonella flagella *in vitro* *J. Mol. Biol.* **106** 167–86

[11] Kamiya R and Asakura S 1977 Flagellar transformations at alkaline pH *J. Mol. Biol.* **108** 513–8

[12] Darnton N and Berg H 2007 Force-extension measurements on bacterial flagella: triggering polymorphic transformations *Biophys. J.* **92** 2230–6

[13] Vogel R and Stark H 2010 Force-extension curves of bacterial flagella *Eur. Phys. J.* E **33** 259–71

[14] Asakura S 1970 Polymerization of flagellin and polymorphism of flagella *Adv. Biophys.* **1** 99–155

[15] Calladine C 1975 Construction of bacterial flagella *Nature* **255** 121–4

[16] Calladine C 1976 Design requirements for the construction of bacterial flagella *J. Theor. Biol.* **57** 469–89

[17] Hasegawa K, Yamashita I and Namba K 1998 Quasi- and nonequivalence in the structure of bacterial flagellar filament *Biophys. J.* **74** 569–75

[18] Srigiriraju S and Powers T 2005 Continuum model for polymorphism of bacterial flagella *Phys. Rev. Lett.* **94** 248101

[19] Srigiriraju S and Powers T 2006 Model for polymorphic transitions in bacterial flagella *Phys. Rev.* E **73** 011902

[20] Kitao A, Yonekura K, Maki-Yonekura S, Samatey F A, Imada K, Namba K and Go N 2006 Switch interactions control energy frustration and multiple flagellar filament structures *Proc. Natl Acad. Sci. USA* **103** 4894–9

[21] Arkhipov A, Freddolino P, Imada K, Namba K and Schulten K 2006 Coarse-grained molecular dynamics simulations of a rotating bacterial flagellum *Biophys. J.* **91** 4589–97

[22] Spagnolie S E and Lauga E 2011 Comparative hydrodynamics of bacterial polymorphism *Phys. Rev. Lett.* **106** 058103

[23] Wada H and Netz R R 2008 Discrete elastic model for stretching-induced flagellar polymorphs *Europhys. Lett.* **82** 28001

[24] Flory P 1953 *Principles of Polymer Chemistry* (Ithaca, NY: Cornell University Press)

[25] Volkenstein M V 1963 *Configurational Statistics of Polymer Chains* (New York: Wiley Intercience)

[26] Birshtein T M and Ptitsyn O B 1964 *Conformations of Macromolecules* (New York: Wiley)

[27] Zimm B H and Bragg J 1959 Theory of the phase transition between helix and random coil in polypeptide chains *J. Chem. Phys.* **31** 526–35

[28] Bloomfield V A 1999 Statistical thermodynamics of helix-coil transitions in biopolymers *Am. J. Phys.* **67** 1212–5

[29] Teramoto A 2001 Cooperative conformational transitions in linear macromolecules undergoing chiral perturbations *Prog. Polym. Sci.* **26** 667–720

[30] Takano M, Nagayama K and Suyama A 2002 How the all-atom simulation and the Ising-based theory reconcile with each other on the helix-coil transition *J. Biol. Phys.* **28** 155–61

[31] Rice J J, Stolovitzky G, Tu Y H and de Tombe P P 2003 Ising model of cardiac thin filament activation with nearest-neighbor cooperative interactions *Biophys. J.* **84** 897–909

[32] Ferreiro D U, Walczak A M, Komives E A and Wolynes P G 2008 The energy landscapes of repeat-containing proteins: topology, cooperativity, and the folding funnels of one-dimensional architectures *PLoS Comput. Biol.* **4** e1000070

[33] De La Cruz E M and Sept D 2010 The kinetics of cooperative cofilin binding reveals two states of the cofilin-actin filament *Biophys. J.* **98** 1893–901

[34] Calladine C R 2010 New twists for bacterial flagella *Nat. Struct. Mol. Biol.* **17** 395–6

[35] Yonekura K, Maki-Yonekura S and Namba K 2003 Complete atomic model of the bacterial flagellar filament by electron cryomicroscopy *Nature* **424** 643–50

[36] Kamiya R, Asakura S, Wakabayashi K and Namba K 1979 Transition of bacterial flagella from helical to straight forms with different subunit arrangements *J. Mol. Biol.* **131** 725–42

[37] Yamashita I, Hasegawa K, Suzuki H, Vonderviszt F, Mimori-Kiyosue Y and Namba K 1998 Structure and

switching of bacterial flagellar filaments studied by x-ray fiber diffraction *Nat. Struct. Biol.* **5** 125–32
[38] Samatey F A, Imada K, Nagashima S, Vonderviszt F, Kumasaka T, Yamamoto M and Namba K 2001 Structure of the bacterial flagellar protofilament and implications for a switch for supercoiling *Nature* **410** 331–7
[39] Friedrich B 2006 A mesoscopic model for helical bacterial flagella *J. Math. Biol.* **53** 162–78
[40] Maki-Yonekura S, Yonekura K and Namba K 2010 Conformational change of flagellin for polymorphic supercoiling of the flagellar filament *Nat. Struct. Mol. Biol.* **17** 417–22
[41] Kanto S, Okino H, Aizawa S I and Yamaguchi S 1991 Amino acids responsible for flagellar shape are distributed in terminal regions of flagellin *J. Mol. Biol.* **219** 471–80
[42] Speier C and Stark H unpublished